



Measurements of the $\Lambda_b^0 \rightarrow J/\psi \Lambda$ decay amplitudes and the Λ_b^0 polarisation in pp collisions at $\sqrt{s} = 7$ TeV[☆]

LHCb Collaboration

ARTICLE INFO

Article history:

Received 22 February 2013

Received in revised form 16 May 2013

Accepted 17 May 2013

Available online 21 May 2013

Editor: M. Doser

ABSTRACT

An angular analysis of $\Lambda_b^0 \rightarrow J/\psi \Lambda$ decays is performed using a data sample corresponding to 1.0 fb^{-1} collected in pp collisions at $\sqrt{s} = 7$ TeV with the LHCb detector at the LHC. A parity violating asymmetry parameter characterising the $\Lambda_b^0 \rightarrow J/\psi \Lambda$ decay of $0.05 \pm 0.17 \pm 0.07$ and a Λ_b^0 transverse production polarisation of $0.06 \pm 0.07 \pm 0.02$ are measured, where the first uncertainty is statistical and the second systematic.

© 2013 CERN. Published by Elsevier B.V. All rights reserved.

1. Introduction

For Λ_b^0 baryons originating from energetic b -quarks, heavy-quark effective theory (HQET) predicts a large fraction of the transverse b -quark polarisation to be retained after hadronisation [1,2], while the longitudinal polarisation should vanish due to parity conservation in strong interactions. For Λ_b^0 baryons produced in $e^-e^+ \rightarrow Z^0 \rightarrow b\bar{b}$ transitions, a substantial polarisation is measured [3–5], in agreement with the $Z^0 b\bar{b}$ coupling of the Standard Model (SM). There is no previous polarisation measurement for Λ_b^0 baryons produced at hadron colliders. The transverse polarisation is estimated to be $\mathcal{O}(10\%)$ in Ref. [6] while Ref. [7] mentions it could be as large as 20%. However, for Λ baryons produced in fixed-target experiments [8–10], the polarisation was observed to depend strongly on the Feynman variable $x_F = 2p_L/\sqrt{s}$, p_L being the Λ longitudinal momentum and \sqrt{s} the collision centre-of-mass energy, and to vanish at $x_F \approx 0$. Extrapolating these results and taking into account the very small $x_F \approx 0.02$ value for Λ_b^0 produced at the Large Hadron Collider (LHC) at $\sqrt{s} = 7$ TeV, this could imply a polarisation much smaller than 10%.

In this Letter, we perform an angular analysis of $\Lambda_b^0 \rightarrow J/\psi(\rightarrow \mu^+\mu^-)\Lambda(\rightarrow p\pi^-)$ decays using 1.0 fb^{-1} of pp collision data collected in 2011 with the LHCb detector [11] at the LHC at $\sqrt{s} = 7$ TeV. Owing to the well-measured $\Lambda \rightarrow p\pi^-$ decay asymmetry parameter (α_Λ) [12] and the known behaviour of the decay of a vector particle into two leptons, the final state angular distribution contains sufficient information to measure the Λ_b^0 production polarisation and the decay amplitudes [13]. The asymmetry of the Λ decay ($\alpha_{\bar{\Lambda}}$) is much less precisely measured [12], however by neglecting possible CP violation effects, which are predicted to be very small in the SM [14,15], α_Λ and $-\alpha_{\bar{\Lambda}}$ can be assumed to

Table 1
Theoretical predictions for the $\Lambda_b^0 \rightarrow J/\psi \Lambda$ decay asymmetry parameter α_b .

Method	Value	Reference
Factorisation	−0.1	[16]
Factorisation	−0.18	[17]
Covariant oscillator quark model	−0.208	[18]
Perturbative QCD	−0.17 to −0.14	[19]
Factorisation (HQET)	0.777	[7]
Light front quark model	−0.204	[20]

be equal. Similarly, CP violation effects in Λ_b^0 decays are neglected, and the decay amplitudes of the Λ_b^0 and $\bar{\Lambda}_b^0$ are therefore assumed to be equal. Inclusion of charge-conjugated modes is henceforth implied. The asymmetry parameter α_b in $\Lambda_b^0 \rightarrow J/\psi \Lambda$ decays, defined in Section 2, is calculated in many publications as summarised in Table 1. Most predictions lie in the range from −21% to −10% while Ref. [7] obtains a large positive value using HQET. Note that the theoretical predictions depend on the calculations of the form-factors and experimental input that were available at the time they were made.

It should be noted that Λ_b^0 baryons can also be produced in the decay of heavier b baryons [21–23], where the polarisation is partially diluted [6]. These strong decays are experimentally difficult to distinguish from Λ_b^0 that hadronise directly from a pp collision and therefore contribute to the measurement presented in this study.

A sufficiently large Λ_b^0 polarisation would allow the photon helicity in $\Lambda_b^0 \rightarrow \Lambda\gamma$ and $\Lambda_b^0 \rightarrow \Lambda^*\gamma$ decays to be probed [6,24,25]. The photon helicity is sensitive to contributions from beyond the SM.

2. Angular formalism

The Λ_b^0 spin has not yet been measured but the quark model prediction is spin $\frac{1}{2}$. The $\Lambda_b^0 \rightarrow J/\psi \Lambda$ mode is therefore the decay

☆ © CERN for the benefit of the LHCb Collaboration.

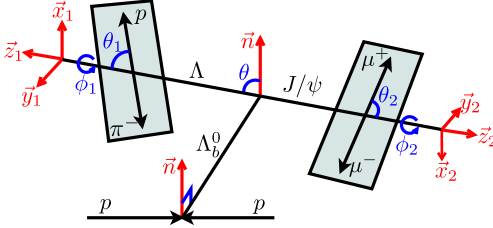


Fig. 1. Definition of the five angles used to describe the $\Lambda_b^0 \rightarrow J/\psi(\rightarrow \mu^+\mu^-)\Lambda(\rightarrow p\pi^-)$ decay.

of a spin $\frac{1}{2}$ particle into a spin 1 and a spin $\frac{1}{2}$ particle. In the helicity formalism, the decay can be described by four $\mathcal{M}_{\lambda_1\lambda_2}$ helicity amplitudes ($\mathcal{M}_{+\frac{1}{2},0}$, $\mathcal{M}_{-\frac{1}{2},0}$, $\mathcal{M}_{-\frac{1}{2},-1}$ and $\mathcal{M}_{+\frac{1}{2},+1}$) where λ_1 (λ_2) is the helicity of the Λ (J/ψ) particle. The angular distribution of the decay ($\frac{d\Gamma}{d\Omega_5}$) is calculated in Ref. [13] and reported in Ref. [26]. It depends on the five angles shown in Fig. 1. The first angle, θ , is the polar angle of the Λ momentum in the Λ_b^0 rest-frame with respect to $\vec{n} = (\vec{p}_{\Lambda_b^0} \times \vec{p}_{\text{beam}})/|\vec{p}_{\Lambda_b^0} \times \vec{p}_{\text{beam}}|$, a unit vector perpendicular to the production plane. The second and third angles are θ_1 and ϕ_1 , the polar and azimuthal angles of the proton in the Λ rest-frame and calculated in the coordinate system defined by $\vec{z}_1 = \vec{p}_\Lambda/|\vec{p}_\Lambda|$ and $\vec{y}_1 = (\vec{n} \times \vec{p}_\Lambda)/|\vec{n} \times \vec{p}_\Lambda|$. The remaining angles are θ_2 and ϕ_2 , the polar and azimuthal angles of the positively-charged muon in the J/ψ rest-frame and calculated in the coordinate system defined by $\vec{z}_2 = \vec{p}_{J/\psi}/|\vec{p}_{J/\psi}|$ and $\vec{y}_2 = (\vec{n} \times \vec{p}_{J/\psi})/|\vec{n} \times \vec{p}_{J/\psi}|$. The angular distribution also depends on the four $\mathcal{M}_{\lambda_1\lambda_2}$ amplitudes, on the α_Λ parameter, and on the transverse polarisation parameter P_b , the projection of the Λ_b^0 polarisation vector on \vec{n} .

Assuming that the detector acceptance over ϕ_1 and ϕ_2 is uniformly distributed, the analysis can be simplified by integrating over the two azimuthal angles

$$\begin{aligned} & \frac{d\Gamma}{d\Omega_5}(\cos\theta, \cos\theta_1, \cos\theta_2) \\ &= \int_{-\pi}^{\pi} \int_{-\pi}^{\pi} \frac{d\Gamma}{d\Omega_5}(\theta, \theta_1, \theta_2, \phi_1, \phi_2) d\phi_1 d\phi_2 \\ &= \frac{1}{16\pi} \sum_{i=0}^7 f_i(|\mathcal{M}_{+\frac{1}{2},0}|^2, |\mathcal{M}_{-\frac{1}{2},0}|^2, |\mathcal{M}_{-\frac{1}{2},-1}|^2, |\mathcal{M}_{+\frac{1}{2},+1}|^2) \\ & \quad \times g_i(P_b, \alpha_\Lambda) h_i(\cos\theta, \cos\theta_1, \cos\theta_2). \end{aligned} \quad (1)$$

The functions describing the decay only depend on the magnitudes of the $\mathcal{M}_{\lambda_1\lambda_2}$ amplitudes, on P_b and α_Λ , and on $\cos\theta$, $\cos\theta_1$, and $\cos\theta_2$. Using the normalisation condition $|\mathcal{M}_{+\frac{1}{2},0}|^2 + |\mathcal{M}_{-\frac{1}{2},0}|^2 + |\mathcal{M}_{-\frac{1}{2},-1}|^2 + |\mathcal{M}_{+\frac{1}{2},+1}|^2 = 1$, the f_i functions can be written in terms of the following three parameters: $\alpha_b \equiv |\mathcal{M}_{+\frac{1}{2},0}|^2 - |\mathcal{M}_{-\frac{1}{2},0}|^2 + |\mathcal{M}_{-\frac{1}{2},-1}|^2 - |\mathcal{M}_{+\frac{1}{2},+1}|^2$, $r_0 \equiv |\mathcal{M}_{+\frac{1}{2},0}|^2 + |\mathcal{M}_{-\frac{1}{2},0}|^2$ and $r_1 \equiv |\mathcal{M}_{+\frac{1}{2},0}|^2 - |\mathcal{M}_{-\frac{1}{2},0}|^2$. The functions used to describe the angular distributions are shown in Table 2. Four parameters (P_b , α_b , r_0 and r_1) have to be measured simultaneously from the angular distribution. The α_b parameter is the parity violating asymmetry characterising the $\Lambda_b^0 \rightarrow J/\psi \Lambda$ decay.

3. Detector, trigger and simulation

The LHCb detector [11] is a single-arm forward spectrometer covering the pseudorapidity range $2 < \eta < 5$, designed for the study of particles containing b - or c -quarks. The detector includes a high precision tracking system consisting of a silicon-

Table 2
Functions used to describe the angular distributions in three dimensions.

i	$f_i(\alpha_b, r_0, r_1)$	$g_i(P_b, \alpha_\Lambda)$	$h_i(\cos\theta, \cos\theta_1, \cos\theta_2)$
0	1	1	1
1	α_b	P_b	$\cos\theta$
2	$2r_1 - \alpha_b$	α_Λ	$\cos\theta_1$
3	$2r_0 - 1$	$P_b \alpha_\Lambda$	$\cos\theta \cos\theta_1$
4	$\frac{1}{2}(1 - 3r_0)$	1	$\frac{1}{2}(3 \cos^2\theta_2 - 1)$
5	$\frac{1}{2}(\alpha_b - 3r_1)$	P_b	$\frac{1}{2}(3 \cos^2\theta_2 - 1) \cos\theta$
6	$-\frac{1}{2}(\alpha_b + r_1)$	α_Λ	$\frac{1}{2}(3 \cos^2\theta_2 - 1) \cos\theta_1$
7	$-\frac{1}{2}(1 + r_0)$	$P_b \alpha_\Lambda$	$\frac{1}{2}(3 \cos^2\theta_2 - 1) \cos\theta \cos\theta_1$

strip vertex detector (VELO) surrounding the pp interaction region, a large-area silicon-strip detector located upstream of a dipole magnet with a bending power of about 4 Tm, and three stations of silicon-strip detectors and straw drift tubes placed downstream. The combined tracking system provides a momentum measurement with relative uncertainty that varies from 0.4% at 5 GeV/c to 0.6% at 100 GeV/c, and three-dimensional impact parameter (IP) resolution of 20 μm for tracks with high transverse momentum. Charged hadrons are identified using two ring-imaging Cherenkov detectors (RICH) [27]. Photon, electron and hadron candidates are identified by a calorimeter system consisting of scintillating-pad and preshower detectors, an electromagnetic calorimeter and a hadronic calorimeter. Muons are identified by a system composed of alternating layers of iron and multiwire proportional chambers [28]. The trigger [29] consists of a hardware stage, based on information from the calorimeter and muon systems, followed by a software stage, which applies a full event reconstruction.

The hardware trigger selects events containing a muon with a transverse momentum, $p_T > 1.48$ GeV/c or two muons with a product of their p_T larger than $(1.3 \text{ GeV/c})^2$. In the subsequent software trigger, we require two oppositely-charged muons having an invariant mass larger than $2800 \text{ MeV}/c^2$ and originating from the same vertex, or a single muon with $p_T > 1.3$ GeV/c and being significantly displaced with respect to all the primary pp interaction vertices (PVs) in the event, or a single muon with $p > 10$ GeV/c and $p_T > 1.7$ GeV/c. Displaced muons are identified by means of their IP and χ_{IP}^2 , where the χ_{IP}^2 is the χ^2 difference when the PV is fitted with or without the muon track. Finally, we require two oppositely-charged muons with an invariant mass within $120 \text{ MeV}/c^2$ of the nominal J/ψ mass [12] forming a common vertex which is significantly displaced from the PVs. Displaced J/ψ vertices are identified by computing the vertex separation χ^2 , the χ^2 difference between the PV and the J/ψ vertex. In the $\Lambda_b^0 \rightarrow J/\psi \Lambda$ selection described below, we use the muon pairs selected by the trigger.

Simulation is used to understand the detector efficiencies and resolutions and to train the analysis procedure. Proton–proton collisions are generated using PYTHIA 6.4 [30] with a specific LHCb configuration [31]. Decays of hadronic particles are described by EvtGen [32] in which final state radiation is generated using Photos [33]. The interaction of the generated particles with the detector and its response are implemented using the GEANT4 toolkit [34] as described in Ref. [35].

4. Signal selection and background rejection

A first set of loose requirements is applied to select $\Lambda_b^0 \rightarrow J/\psi \Lambda$ decays. Charged tracks are identified as either protons or pions using information provided by the RICH system. Candidate Λ baryons are reconstructed from oppositely-charged proton and pion candidates. They are reconstructed either when the Λ decays

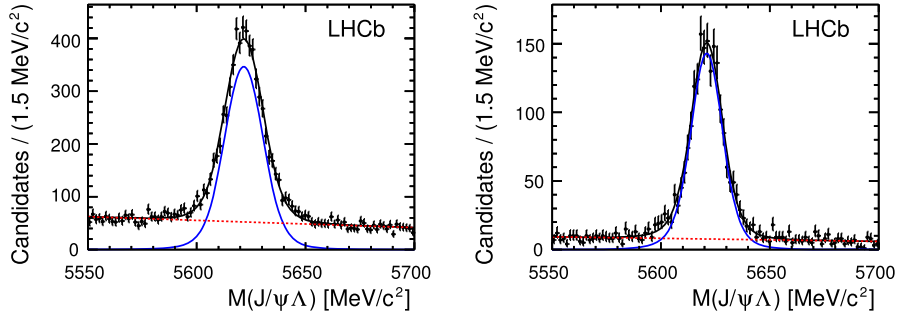


Fig. 2. Mass distribution for the $\Lambda_b^0 \rightarrow J/\psi \Lambda$ mode for the (left) downstream and (right) long candidates. The fitted signal component is shown as a solid blue curve while the background component is shown as a dashed red line.

within the VELO (“long Λ ”), or when the decay occurs outside the VELO acceptance (“downstream Λ ”). The latter category increases the acceptance significantly for long-lived Λ decays. In both cases, the two tracks are required to have $p > 2$ GeV/c, to be well separated from the PVs and to originate from a common vertex. In addition, protons are required to have $p_T > 0.5$ GeV/c and pions to have $p_T > 0.1$ GeV/c. Finally, the invariant mass of the Λ candidates is required to be within 15 MeV/c² of the nominal Λ mass [12]. To form J/ψ candidates, two oppositely-charged muons with $p_T(\mu) > 0.5$ GeV/c are combined and their invariant mass is required to be within 80 MeV/c² of the nominal J/ψ mass. Subsequently, Λ_b^0 candidates are formed by combining the Λ and J/ψ candidates. To improve the Λ_b^0 mass resolution, the muons from the J/ψ decay are constrained to come from a common point and to have an invariant mass equal to the J/ψ mass. We constrain the Λ and J/ψ candidates to originate from a common vertex and to have an invariant mass between 5120 and 6120 MeV/c². Moreover, Λ_b^0 candidates must have their momenta pointing to the associated PV by requiring $\cos\theta_d > 0.99$ where θ_d is the angle between the Λ_b^0 momentum vector and the direction from the PV to the Λ_b^0 vertex. The associated PV is the PV having the smallest χ_{IP}^2 value.

To reduce the combinatorial background, a multivariate selection based on a boosted decision tree (BDT) [36,37] with eight variables is used. Five variables are related to the Λ_b^0 candidate: $\cos\theta_d$, the χ_{IP}^2 , the proper decay time, the vertex χ^2 and the vertex separation χ^2 between the PV and the vertex. Here, the vertex separation χ^2 is the difference in χ^2 between the nominal vertex fit and a vertex fit where the Λ_b^0 is assumed to have zero lifetime. The proper decay time is the distance between the associated PV and the Λ_b^0 decay vertex divided by the Λ_b^0 momentum. Two variables are related to the J/ψ candidate: the vertex χ^2 and the invariant mass of the two muons. The last variable used in the BDT is the invariant mass of the Λ candidate. The BDT is using simulation for signal and sideband data ($M(J/\psi \Lambda) > 5800$ MeV/c²) for background in its training. The optimal BDT requirement is found separately for downstream and long candidates by maximising the signal significance $N_{\text{sig}}/\sqrt{N_{\text{sig}} + N_{\text{bkg}}}$, where N_{sig} and N_{bkg} are the expected signal and background yields in a tight signal region around the Λ_b^0 mass. These two yields are estimated using the signal and background yields measured in data after the first set of loose requirements and using the BDT efficiency measured with the training samples. The BDT selection keeps about 90% of the signal while removing about 80% (90%) of the background events for the downstream (long) candidates. Less background is rejected in the downstream case due to larger contamination from misreconstructed $B^0 \rightarrow J/\psi K_S^0$ background decays. Candidates with $5550 < M(J/\psi \Lambda) < 5700$ MeV/c² are used for the final analysis. In this mass range, the $B^0 \rightarrow J/\psi K_S^0$ back-

ground is found to have a similar shape as the combinatorial background.

5. Fitting procedure

An unbinned extended maximum likelihood fit to the mass distribution of the Λ_b^0 candidates is performed. The likelihood function is defined as

$$\mathcal{L}_{\text{mass}} = \frac{e^{-\sum_j N_j}}{N!} \times \prod_{i=1}^N \left(\sum_j N_j P_j(M_i(J/\psi \Lambda)) \right), \quad (2)$$

where i runs over the events, j runs over the different signal and background probability density functions (PDF), N_j are the yields and P_j the PDFs. The sum of two Crystal Ball functions [38] with opposite side tails and common mean and width parameters is used to describe the signal mass distribution. The mean and width parameters are left free in the fit while the other parameters are taken from the simulated signal sample. The background is modelled with a first-order polynomial function. The candidates reconstructed from downstream and long Λ combinations are fitted separately taking into account that the resolution is worse for the downstream signal candidates. The results of the fits to the mass distributions are shown in Fig. 2. We obtain 5346 ± 96 (5189 ± 95) downstream and 1861 ± 49 (761 ± 36) long signal (background) candidates. Using the results of this fit, *sWeights* (w_{mass}) are computed by means of the *sPlot* technique [39], in order to statistically subtract the background in the angular distribution.

To ensure accurate modelling of the signal, corrections to the p_T and rapidity (y) spectra are obtained by comparing the simulation with data by means of the *sPlot* technique. For the Λ_b^0 and Λ particles, the simulated data is corrected using two-dimensional (p_T, y) distributions in order to better reproduce the data. These distributions do not depend on the polarisation and the decay amplitudes but have an impact on the reconstruction acceptance. The same procedure is used on the pion of $B^0 \rightarrow J/\psi K_S^0$ decays and is subsequently used to calibrate the (p_T, y) spectrum of the pion of the $\Lambda_b^0 \rightarrow J/\psi \Lambda$ decay.

Since the detector acceptance depends on the three decay angles, the acceptance is modelled with a sum of products of Legendre polynomials (L_i)

$$f_{\text{acc}} = \sum_{i,j,k} c_{ijk} L_i(\cos\theta) L_j(\cos\theta_1) L_k(\cos\theta_2), \quad (3)$$

where i and k are chosen to be even or equal to one. Unbinned maximum likelihood fits to the simulated signal candidates are performed, separately for downstream and long candidates. The simulated is produced using a phase-space model and unpolarised

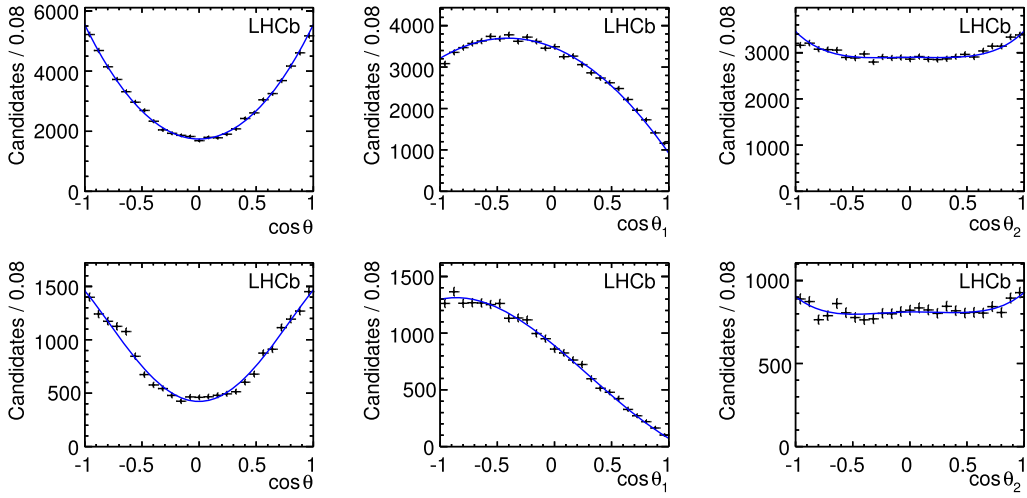


Fig. 3. Projections of the acceptance function together with the simulated signal data for (top) downstream and (bottom) long candidates.

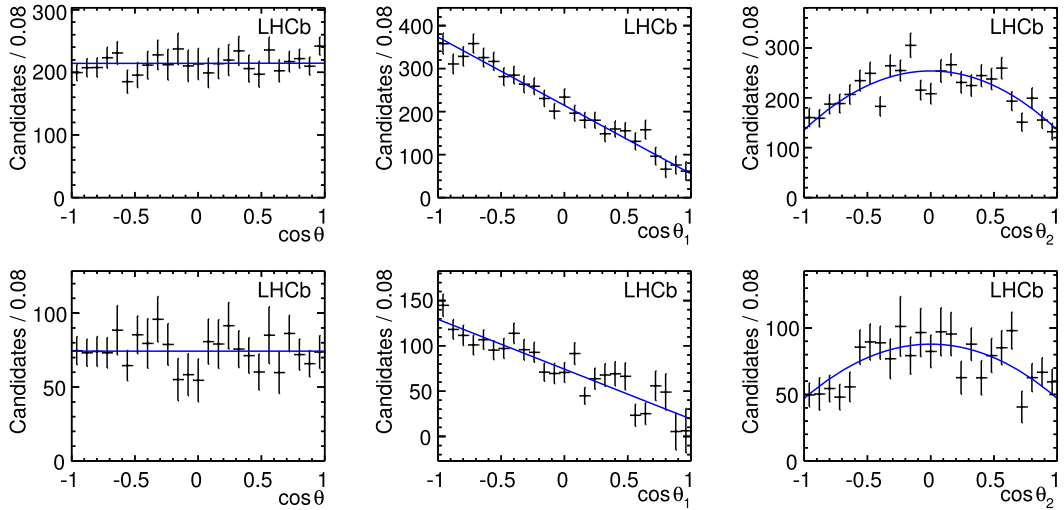


Fig. 4. Projections of the angular distribution of the background subtracted and acceptance corrected $\Lambda_b^0 \rightarrow J/\psi \Lambda$ data for the (top) downstream and (bottom) long candidates. The fit is shown as solid lines.

Λ_b^0 baryons. The three angular distributions are therefore uniformly generated. Acceptances of the Λ_b^0 and $\bar{\Lambda}_b^0$ decays are found to be statistically consistent. A common acceptance function is therefore used. The maximum orders of the Legendre polynomials are chosen by comparing the fit probability. The requirements $i < 5$, $j < 4$, $k < 5$ and $i + j + k < 9$ are chosen. The results of the fit to the acceptance distributions are shown in Fig. 3.

We then perform an unbinned likelihood fit to the $(\cos\theta, \cos\theta_1, \cos\theta_2)$ distribution. Each candidate is weighted with $w_{\text{tot}} = w_{\text{mass}} \times w_{\text{acc}}$ where w_{mass} subtracts the background and $w_{\text{acc}} = 1/f_{\text{acc}}(\cos\theta, \cos\theta_1, \cos\theta_2)$ corrects for the angular acceptance [40]. The sum of the w_{mass} weights over all the events is by construction equal to the signal yield, and w_{tot} is normalised in the same way. Since the weighting procedure performs background subtraction and corrects for acceptance effects, only the signal PDF has to be included in the fit of the angular distribution. The detector resolution is neglected in the nominal fit as it is found to have little effect on the results. It will be considered as source of systematic uncertainty. The likelihood is therefore

$$\mathcal{L}_{\text{ang}} = \prod_{i=1}^N w_{\text{tot}}^i \frac{d\Gamma}{d\Omega_3}(\cos\theta^i, \cos\theta_1^i, \cos\theta_2^i), \quad (4)$$

where i runs over all events. A simultaneous fit to the angular distributions of the downstream and long samples is performed. The α_Λ parameter is fixed to its measured value, 0.642 ± 0.013 [12].

The accurate modelling of the acceptance is checked with a similar decay, $B^0 \rightarrow J/\psi K_S^0$. Here, the angular distribution is known, and B^0 mesons are unpolarised. These decays are selected in the same way as signal, and the fitting procedure described above is performed. Agreement with the expected $(\cos\theta, \cos\theta_1, \cos\theta_2)$ distribution is obtained.

6. Results

The results of the fits to the angular distributions of the weighted $\Lambda_b^0 \rightarrow J/\psi \Lambda$ data are shown in Fig. 4. We obtain the following results: $P_b = 0.06 \pm 0.06$, $\alpha_b = 0.00 \pm 0.10$, $r_0 = 0.58 \pm 0.02$ and $r_1 = -0.58 \pm 0.06$, where the uncertainties are statistical only.

The polarisation could be different between Λ_b^0 and $\bar{\Lambda}_b^0$ due to their respective production mechanisms. The data are separated according to the Λ_b^0 flavour and fitted using the same amplitude parameters but different parameters for the Λ_b^0 and $\bar{\Lambda}_b^0$ polarisations. As compatible results are obtained within statistical uncer-

Table 3

Absolute systematic uncertainties on the measured parameters.

Source	P_b	α_b	r_0	r_1
Acceptance	0.02	0.04	0.006	0.03
Simulated data calibration	0.01	0.04	0.006	0.03
Fit bias	0.004	0.04	0.001	0.02
Angular resolution	0.002	0.01	< 0.001	0.005
Background subtraction	0.001	0.006	0.001	0.005
α_A	0.002	< 0.001	< 0.001	0.01
Total (quadratic sum)	0.02	0.07	0.01	0.05

tainties, the polarisations of Λ_b^0 and $\bar{\Lambda}_b^0$ baryons are assumed to be equal.

A possible bias is investigated by fitting samples of generated experiments with sizes and parameters close to those measured in data. We generate many samples varying α_b between -0.25 to 0.25 while keeping r_0 equal to $-r_1$, thus keeping $|\mathcal{M}_{+\frac{1}{2},+1}|^2$ and $|\mathcal{M}_{+\frac{1}{2},0}|^2$ equal to zero. We find that the fitting procedure biases all parameters toward negative values, slightly for P_b and r_0 ($\sim 10\%$ of their respective statistical uncertainties) and more significantly for α_b and r_1 ($\sim 40\%$ of their respective statistical uncertainties). For P_b and r_0 , the biases do not change significantly when changing the value of α_b used to generate the simulated samples. On the other hand, the biases on α_b and r_1 do change, and the observed discrepancies are treated as systematic uncertainties. Moreover, the statistical uncertainties on the four fit parameters are underestimated: again slightly for P_b and r_0 and significantly, by a factor of ~ 1.7 , for α_b and r_1 .

We correct the measured values and statistical uncertainties of the four fit parameters. The corrected statistical uncertainties are obtained by multiplying the covariance matrix with a correction matrix obtained from the study of the simulated samples. This correction matrix contains on its diagonal the squares of the widths of the pull distributions of the four fit parameters. The remaining entries of this matrix are set to zero as the correlation matrix computed with the results of the fits of the generated samples is found to be very close to the correlation matrix calculated when fitting the data.

Finally, the corrected result is $P_b = 0.06 \pm 0.07$, $\alpha_b = 0.05 \pm 0.17$, $r_0 = 0.58 \pm 0.02$, $r_1 = -0.56 \pm 0.10$, where the uncertainties are statistical only. The corrected statistical correlation matrix between the four fit parameters (P_b, α_b, r_0, r_1) is

$$\begin{pmatrix} 1 & 0.10 & -0.07 & 0.13 \\ & 1 & -0.63 & 0.95 \\ & & 1 & -0.56 \\ & & & 1 \end{pmatrix}.$$

Large correlations are not seen between the polarisation and the amplitude parameters. On the other hand, the amplitude parameters are strongly correlated with respect to each other, α_b and r_1 being almost fully correlated.

7. Systematic uncertainties and significance

The systematic uncertainty on each measured physics parameter is evaluated by repeating the fit to the data varying its input parameters assuming Gaussian distributions and taking into account correlations when possible. The systematic uncertainties are summarised in Table 3. They are dominated by the uncertainty arising from the acceptance function, the calibration of the simulated signal sample and the fit bias. The uncertainty related to the acceptance function is obtained by varying the coefficients of the Legendre function within their uncertainties and taking into account their correlations. For the calibration of our simulated data,

the uncertainty is obtained when changing the (p_T, y) calibrations of the Λ_b^0 , Λ and pion particles within their uncertainties and obtaining a new acceptance function. The function that is used to fit the data does not include the effect of the angular resolution. The angular resolution, obtained with simulated samples, is negligible for θ and θ_2 . However, it is large, up to $\sim 70\%$, for small values of θ_1 . The systematic uncertainty is obtained by fitting simulated samples in which the resolution effect is introduced. Effects of the deviation from an uniform acceptance in ϕ_1 and ϕ_2 assumed in Eq. (1) are found to be negligible. The simplification to use only one component to describe the background is found not to bias the result. Other systematic uncertainties are small or negligible. These are related to the signal mass PDF parameters, the background subtraction and α_A . The uncertainty related to the background subtraction are obtained when varying the obtained result of the mass fit and computing the w_{mass} weights again. The α_A parameter is varied within its measurement uncertainties [12].

To compare our results with a prediction on a parameter p , we compute the significance with respect to a p_{test} value using a profile along p of the likelihood function, *i.e.* the likelihood value obtained when varying p and minimising with respect to the other parameters. A Monte Carlo integration is performed to include the systematic uncertainties in the likelihood profiles. We perform the fit to the data when varying all systematic uncertainties and obtain a likelihood profile for each fit of the data. The likelihood profile which includes all systematic uncertainties is then the average of all the obtained profiles. The significance is defined as $S(p = p_{\text{test}}) = \sqrt{2(\log \mathcal{L}(p_{\text{test}}) - \log \mathcal{L}(p_0))}$, where $\mathcal{L}(p_0)$ is the likelihood value of the nominal fit. Significances are given in the concluding section of this Letter.

8. Conclusion

We have performed an angular analysis of about 7200 $\Lambda_b^0 \rightarrow J/\psi (\rightarrow \mu^+ \mu^-) \Lambda (\rightarrow p \pi^-)$ decays. The $\Lambda_b^0 \rightarrow J/\psi \Lambda$ decay amplitudes are measured for the first time, and the Λ_b^0 production polarisation for the first time at a hadron collider. The results are

$$P_b = 0.06 \pm 0.07 \pm 0.02,$$

$$\alpha_b = 0.05 \pm 0.17 \pm 0.07,$$

$$r_0 = 0.58 \pm 0.02 \pm 0.01,$$

$$r_1 = -0.56 \pm 0.10 \pm 0.05,$$

which correspond to the four helicity amplitudes

$$|\mathcal{M}_{+\frac{1}{2},0}|^2 = 0.01 \pm 0.04 \pm 0.03,$$

$$|\mathcal{M}_{-\frac{1}{2},0}|^2 = 0.57 \pm 0.06 \pm 0.03,$$

$$|\mathcal{M}_{-\frac{1}{2},-1}|^2 = 0.51 \pm 0.05 \pm 0.02,$$

$$|\mathcal{M}_{+\frac{1}{2},+1}|^2 = -0.10 \pm 0.04 \pm 0.03,$$

where the first uncertainty is statistical and the second systematic. The reported polarisation and amplitudes are obtained for the combination of Λ_b^0 and $\bar{\Lambda}_b^0$ decays. More data are required to probe any possible difference.

Our result cannot exclude a transverse polarisation at the order of 10% [6]. However, a value of 20% as mentioned in Ref. [7] is disfavoured at the level of 2.7 standard deviations.

For the Λ_b^0 asymmetry parameter, our result is compatible with the predictions ranging from -21% to -10% [16–20] but does not agree with the HQET prediction of 77.7% [7] at 5.8 standard deviations.

Acknowledgements

We express our gratitude to our colleagues in the CERN accelerator departments for the excellent performance of the LHC. We thank the technical and administrative staff at the LHCb institutes. We acknowledge support from CERN and from the national agencies: CAPES, CNPq, FAPERJ and FINEP (Brazil); NSFC (China); CNRS/IN2P3 and Region Auvergne (France); BMBF, DFG, HGF and MPG (Germany); SFI (Ireland); INFN (Italy); FOM and NWO (The Netherlands); SCSR (Poland); ANCS/IFA (Romania); MinES, Rosatom, RFBR and NRC “Kurchatov Institute” (Russia); MinECo, XuntaGal and GENCAT (Spain); SNSF and SER (Switzerland); NAS Ukraine (Ukraine); STFC (United Kingdom); NSF (USA). We also acknowledge the support received from the ERC under FP7. The Tier1 computing centres are supported by IN2P3 (France), KIT and BMBF (Germany), INFN (Italy), NWO and SURF (The Netherlands), PIC (Spain), GridPP (United Kingdom). We are thankful for the computing resources put at our disposal by Yandex LLC (Russia), as well as to the communities behind the multiple open source software packages that we depend on.

Open access

This article is published Open Access at sciedirect.com. It is distributed under the terms of the Creative Commons Attribution License 3.0, which permits unrestricted use, distribution, and reproduction in any medium, provided the original authors and source are credited.

References

- [1] T. Mannel, G.A. Schuler, Phys. Lett. B 279 (1992) 194.
- [2] A.F. Falk, M.E. Peskin, Phys. Rev. D 49 (1994) 3320, arXiv:hep-ph/9308241.
- [3] ALEPH Collaboration, D. Buskulic, et al., Phys. Lett. B 365 (1996) 437.
- [4] OPAL Collaboration, G. Abbiendi, et al., Phys. Lett. B 444 (1998) 539, arXiv:hep-ex/9808006.
- [5] DELPHI Collaboration, P. Abreu, et al., Phys. Lett. B 474 (2000) 205.
- [6] G. Hiller, M. Knecht, F. Legger, T. Schietinger, Phys. Lett. B 649 (2007) 152, arXiv:hep-ph/0702191.
- [7] Z.J. Ajaltouni, E. Conte, O. Leitner, Phys. Lett. B 614 (2005) 165, arXiv:hep-ph/0412116.
- [8] E799 Collaboration, E.J. Ramberg, et al., Phys. Lett. B 338 (1994) 403.
- [9] NA48 Collaboration, V. Fanti, et al., Eur. Phys. J. C 6 (1999) 265.
- [10] HERA-B Collaboration, I. Abt, et al., Phys. Lett. B 638 (2006) 415, arXiv:hep-ex/0603047.
- [11] LHCb Collaboration, A.A. Alves Jr., et al., JINST 3 (2008) S08005.
- [12] Particle Data Group, J. Beringer, et al., Phys. Rev. D 86 (2012) 010001.
- [13] R. Lednický, Sov. J. Nucl. Phys. 43 (1986) 817.
- [14] J.F. Donoghue, X.-G. He, S. Pakvasa, Phys. Rev. D 34 (1986) 833.
- [15] J.F. Donoghue, B.R. Holstein, G. Valencia, Phys. Lett. B 178 (1986) 319.
- [16] H.-Y. Cheng, Phys. Rev. D 56 (1997) 2799, arXiv:hep-ph/9612223.
- [17] Fayyazuddin, Riazuddin, Phys. Rev. D 58 (1998) 014016, arXiv:hep-ph/9802326.
- [18] R. Mohanta, et al., Prog. Theor. Phys. 101 (1999) 959, arXiv:hep-ph/9904324.
- [19] C.-H. Chou, H.-H. Shih, S.-C. Lee, H.-n. Li, Phys. Rev. D 65 (2002) 074030, arXiv:hep-ph/0112145.
- [20] Z.-T. Wei, H.-W. Ke, X.-Q. Li, Phys. Rev. D 80 (2009) 094016, arXiv:0909.0100.
- [21] CDF Collaboration, T. Aaltonen, et al., Phys. Rev. Lett. 99 (2007) 202001, arXiv:0706.3868.
- [22] CDF Collaboration, T. Aaltonen, et al., Phys. Rev. D 85 (2012) 092011, arXiv:1112.2808.
- [23] LHCb Collaboration, R. Aaij, et al., Phys. Rev. Lett. 109 (2012) 172003, arXiv:1205.3452.
- [24] T. Mannel, S. Recksiegel, J. Phys. G 24 (1998) 979, arXiv:hep-ph/9701399.
- [25] F. Legger, T. Schietinger, Phys. Lett. B 645 (2007) 204, arXiv:hep-ph/0605245.
- [26] J. Hrivnac, R. Lednický, M. Smizanska, J. Phys. G 21 (1995) 629, arXiv:hep-ph/9405231.
- [27] M. Adinolfi, et al., Eur. Phys. J. C (2012), submitted for publication, arXiv:1211.6759.
- [28] A.A. Alves Jr., et al., JINST 8 (2013) P02022, arXiv:1211.1346.
- [29] LHCb Collaboration, R. Aaij, et al., JINST 8 (2013) P04022, arXiv:1211.3055.
- [30] T. Sjöstrand, S. Mrenna, P. Skands, JHEP 0605 (2006) 026, arXiv:hep-ph/0603175.
- [31] I. Belyaev, et al., in: Nuclear Science Symposium Conference Record (NSS/MIC), IEEE (2010) 1155.
- [32] D.J. Lange, Nucl. Instrum. Meth. A 462 (2001) 152.
- [33] P. Golonka, Z. Was, Eur. Phys. J. C 45 (2006) 97, arXiv:hep-ph/0506026.
- [34] GEANT4 Collaboration, J. Allison, et al., IEEE Trans. Nucl. Sci. 53 (2006) 270; GEANT4 Collaboration, S. Agostinelli, et al., Nucl. Instrum. Meth. A 506 (2003) 250.
- [35] M. Clemencic, et al., J. Phys. Conf. Ser. 331 (2011) 032023.
- [36] L. Breiman, J.H. Friedman, R.A. Olshen, C.J. Stone, Classification and Regression Trees, Wadsworth International Group, Belmont, California, USA, 1984.
- [37] R.E. Schapire, Y. Freund, J. Comp. Syst. Sc. 55 (1997) 119.
- [38] T. Skwarnicki, A study of the radiative cascade transitions between the Upsilon-prime and Upsilon resonances, PhD thesis, Institute of Nuclear Physics, Krakow, 1986, DESY-F31-86-02.
- [39] M. Pivk, F.R. Le Diberder, Nucl. Instrum. Methods Phys. Res. A 555 (2005) 356, arXiv:physics/0402083.
- [40] Y. Xie, sFit: a method for background subtraction in maximum likelihood fit, arXiv:0905.0724.

LHCb Collaboration

- R. Aaij⁴⁰, C. Abellán Beteta^{35,n}, B. Adeva³⁶, M. Adinolfi⁴⁵, C. Adrover⁶, A. Affolder⁵¹, Z. Ajaltouni⁵, J. Albrecht⁹, F. Alessio³⁷, M. Alexander⁵⁰, S. Ali⁴⁰, G. Alkhazov²⁹, P. Alvarez Cartelle³⁶, A.A. Alves Jr.^{24,37}, S. Amato², S. Amerio²¹, Y. Amhis⁷, L. Anderlini^{17,f}, J. Anderson³⁹, R. Andreassen⁵⁹, R.B. Appleby⁵³, O. Aquines Gutierrez¹⁰, F. Archilli¹⁸, A. Artamonov³⁴, M. Artuso⁵⁶, E. Aslanides⁶, G. Auriemma^{24,m}, S. Bachmann¹¹, J.J. Back⁴⁷, C. Baesso⁵⁷, V. Balagura³⁰, W. Baldini¹⁶, R.J. Barlow⁵³, C. Barschel³⁷, S. Barsuk⁷, W. Barter⁴⁶, Th. Bauer⁴⁰, A. Bay³⁸, J. Beddow⁵⁰, F. Bedeschi²², I. Bediaga¹, S. Belogurov³⁰, K. Belous³⁴, I. Belyaev³⁰, E. Ben-Haim⁸, M. Benayoun⁸, G. Bencivenni¹⁸, S. Benson⁴⁹, J. Benton⁴⁵, A. Berezhnoy³¹, R. Bernet³⁹, M.-O. Bettler⁴⁶, M. van Beuzekom⁴⁰, A. Bien¹¹, S. Bifani¹², T. Bird⁵³, A. Bizzeti^{17,h}, P.M. Bjørnstad⁵³, T. Blake³⁷, F. Blanc³⁸, J. Blouw¹¹, S. Blusk⁵⁶, V. Bocci²⁴, A. Bondar³³, N. Bondar²⁹, W. Bonivento¹⁵, S. Borghi⁵³, A. Borgia⁵⁶, T.J.V. Bowcock⁵¹, E. Bowen³⁹, C. Bozzi¹⁶, T. Brambach⁹, J. van den Brand⁴¹, J. Bressieux³⁸, D. Brett⁵³, M. Britsch¹⁰, T. Britton⁵⁶, N.H. Brook⁴⁵, H. Brown⁵¹, I. Burducea²⁸, A. Bursche³⁹, G. Busetto^{21,q}, J. Buytaert³⁷, S. Cadeddu¹⁵, O. Callot⁷, M. Calvi^{20,j}, M. Calvo Gomez^{35,n}, A. Camboni³⁵, P. Campana^{18,37}, A. Carbone^{14,c}, G. Carboni^{23,k}, R. Cardinale^{19,i}, A. Cardini¹⁵, H. Carranza-Mejia⁴⁹, L. Carson⁵², K. Carvalho Akiba², G. Casse⁵¹, M. Cattaneo³⁷, Ch. Cauet⁹, M. Charles⁵⁴, Ph. Charpentier³⁷, P. Chen^{3,38}, N. Chiapolini³⁹, M. Chrzaszcz²⁵, K. Ciba³⁷, X. Cid Vidal³⁶, G. Ciezarek⁵², P.E.L. Clarke⁴⁹, M. Clemencic³⁷, H.V. Cliff⁴⁶, J. Closier³⁷, C. Coca²⁸, V. Coco⁴⁰, J. Cogan⁶, E. Cogneras⁵, P. Collins³⁷, A. Comerma-Montells³⁵, A. Contu¹⁵, A. Cook⁴⁵, M. Coombes⁴⁵, S. Coquereau⁸, G. Corti³⁷, B. Couturier³⁷, G.A. Cowan³⁸,

- D. Craik ⁴⁷, S. Cunliffe ⁵², R. Currie ⁴⁹, C. D'Ambrosio ³⁷, P. David ⁸, P.N.Y. David ⁴⁰, I. De Bonis ⁴, K. De Bruyn ⁴⁰, S. De Capua ⁵³, M. De Cian ³⁹, J.M. De Miranda ¹, M. De Oyanguren Campos ^{35,o}, L. De Paula ², W. De Silva ⁵⁹, P. De Simone ¹⁸, D. Decamp ⁴, M. Deckenhoff ⁹, L. Del Buono ⁸, D. Derkach ¹⁴, O. Deschamps ⁵, F. Dettori ⁴¹, A. Di Canto ¹¹, H. Dijkstra ³⁷, M. Dogaru ²⁸, S. Donleavy ⁵¹, F. Dordei ¹¹, A. Dosil Suárez ³⁶, D. Dossett ⁴⁷, A. Dovbnya ⁴², F. Dupertuis ³⁸, R. Dzhelyadin ³⁴, A. Dziurda ²⁵, A. Dzyuba ²⁹, S. Easo ^{48,37}, U. Egede ⁵², V. Egorychev ³⁰, S. Eidelman ³³, D. van Eijk ⁴⁰, S. Eisenhardt ⁴⁹, U. Eitschberger ⁹, R. Ekelhof ⁹, L. Eklund ⁵⁰, I. El Rifai ⁵, Ch. Elsasser ³⁹, D. Elsby ⁴⁴, A. Falabella ^{14,e}, C. Färber ¹¹, G. Fardell ⁴⁹, C. Farinelli ⁴⁰, S. Farry ¹², V. Fave ³⁸, D. Ferguson ⁴⁹, V. Fernandez Albor ³⁶, F. Ferreira Rodrigues ¹, M. Ferro-Luzzi ³⁷, S. Filippov ³², C. Fitzpatrick ³⁷, M. Fontana ¹⁰, F. Fontanelli ^{19,i}, R. Forty ³⁷, O. Francisco ², M. Frank ³⁷, C. Frei ³⁷, M. Frosini ^{17,f}, S. Furcas ²⁰, E. Furfarò ²³, A. Gallas Torreira ³⁶, D. Galli ^{14,c}, M. Gandelman ², P. Gandini ⁵⁴, Y. Gao ³, J. Garofoli ⁵⁶, P. Garosi ⁵³, J. Garra Tico ⁴⁶, L. Garrido ³⁵, C. Gaspar ³⁷, R. Gauld ⁵⁴, E. Gersabeck ¹¹, M. Gersabeck ⁵³, T. Gershon ^{47,37}, Ph. Ghez ⁴, V. Gibson ⁴⁶, V.V. Gligorov ³⁷, C. Göbel ⁵⁷, D. Golubkov ³⁰, A. Golutvin ^{52,30,37}, A. Gomes ², H. Gordon ⁵⁴, M. Grabalosa Gándara ⁵, R. Graciani Diaz ³⁵, L.A. Granado Cardoso ³⁷, E. Graugés ³⁵, G. Graziani ¹⁷, A. Grecu ²⁸, E. Greening ⁵⁴, S. Gregson ⁴⁶, O. Grünberg ⁵⁸, B. Gui ⁵⁶, E. Gushchin ³², Yu. Guz ³⁴, T. Gys ³⁷, C. Hadjivasiliou ⁵⁶, G. Haefeli ³⁸, C. Haen ³⁷, S.C. Haines ⁴⁶, S. Hall ⁵², T. Hampson ⁴⁵, S. Hansmann-Menzemer ¹¹, N. Harnew ⁵⁴, S.T. Harnew ⁴⁵, J. Harrison ⁵³, T. Hartmann ⁵⁸, J. He ⁷, V. Heijne ⁴⁰, K. Hennessy ⁵¹, P. Henrard ⁵, J.A. Hernando Morata ³⁶, E. van Herwijnen ³⁷, E. Hicks ⁵¹, D. Hill ⁵⁴, M. Hoballah ⁵, C. Hombach ⁵³, P. Hopchev ⁴, W. Hulsbergen ⁴⁰, P. Hunt ⁵⁴, T. Huse ⁵¹, N. Hussain ⁵⁴, D. Hutchcroft ⁵¹, D. Hynds ⁵⁰, V. Iakovenko ⁴³, M. Idzik ²⁶, P. Ilten ¹², R. Jacobsson ³⁷, A. Jaeger ¹¹, E. Jans ⁴⁰, P. Jaton ³⁸, F. Jing ³, M. John ⁵⁴, D. Johnson ⁵⁴, C.R. Jones ⁴⁶, B. Jost ³⁷, M. Kaballo ⁹, S. Kandybei ⁴², M. Karacson ³⁷, T.M. Karbach ³⁷, I.R. Kenyon ⁴⁴, U. Kerzel ³⁷, T. Ketel ⁴¹, A. Keune ³⁸, B. Khanji ²⁰, O. Kochebina ⁷, I. Komarov ^{38,31}, R.F. Koopman ⁴¹, P. Koppenburg ⁴⁰, M. Korolev ³¹, A. Kozlinskiy ⁴⁰, L. Kravchuk ³², K. Kreplin ¹¹, M. Kreps ⁴⁷, G. Krocker ¹¹, P. Krokovny ³³, F. Kruse ⁹, M. Kucharczyk ^{20,25,j}, V. Kudryavtsev ³³, T. Kvaratskheliya ^{30,37}, V.N. La Thi ³⁸, D. Lacarrere ³⁷, G. Lafferty ⁵³, A. Lai ¹⁵, D. Lambert ⁴⁹, R.W. Lambert ⁴¹, E. Lanciotti ³⁷, G. Lanfranchi ^{18,37}, C. Langenbruch ³⁷, T. Latham ⁴⁷, C. Lazzeroni ⁴⁴, R. Le Gac ⁶, J. van Leerdam ⁴⁰, J.-P. Lees ⁴, R. Lefèvre ⁵, A. Leflat ^{31,37}, J. Lefrançois ⁷, S. Leo ²², O. Leroy ⁶, B. Leverington ¹¹, Y. Li ³, L. Li Gioi ⁵, M. Liles ⁵¹, R. Lindner ³⁷, C. Linn ¹¹, B. Liu ³, G. Liu ³⁷, J. von Loeben ²⁰, S. Lohn ³⁷, J.H. Lopes ², E. Lopez Asamar ³⁵, N. Lopez-March ³⁸, H. Lu ³, D. Lucchesi ^{21,q}, J. Luisier ³⁸, H. Luo ⁴⁹, F. Machefert ⁷, I.V. Machikhiliyan ^{4,30}, F. Maciuc ²⁸, O. Maev ^{29,37}, S. Malde ⁵⁴, G. Manca ^{15,d}, G. Mancinelli ⁶, U. Marconi ¹⁴, R. Märki ³⁸, J. Marks ¹¹, G. Martellotti ²⁴, A. Martens ⁸, L. Martin ⁵⁴, A. Martín Sánchez ⁷, M. Martinelli ⁴⁰, D. Martinez Santos ⁴¹, D. Martins Tostes ², A. Massafferri ¹, R. Matev ³⁷, Z. Mathe ³⁷, C. Matteuzzi ²⁰, E. Maurice ⁶, A. Mazurov ^{16,32,37,e}, J. McCarthy ⁴⁴, R. McNulty ¹², A. Mcnab ⁵³, B. Meadows ^{59,54}, F. Meier ⁹, M. Meissner ¹¹, M. Merk ⁴⁰, D.A. Milanes ⁸, M.-N. Minard ⁴, J. Molina Rodriguez ⁵⁷, S. Monteil ⁵, D. Moran ⁵³, P. Morawski ²⁵, M.J. Morello ^{22,s}, R. Mountain ⁵⁶, I. Mous ⁴⁰, F. Muheim ⁴⁹, K. Müller ³⁹, R. Muresan ²⁸, B. Muryn ²⁶, B. Muster ³⁸, P. Naik ⁴⁵, T. Nakada ³⁸, R. Nandakumar ⁴⁸, I. Nasteva ¹, M. Needham ⁴⁹, N. Neufeld ³⁷, A.D. Nguyen ³⁸, T.D. Nguyen ³⁸, C. Nguyen-Mau ^{38,p}, M. Nicol ⁷, V. Niess ⁵, R. Niet ⁹, N. Nikitin ³¹, T. Nikodem ¹¹, A. Nomerotski ⁵⁴, A. Novoselov ³⁴, A. Oblakowska-Mucha ²⁶, V. Obraztsov ³⁴, S. Oggero ⁴⁰, S. Ogilvy ⁵⁰, O. Okhrimenko ⁴³, R. Oldeman ^{15,37,d}, M. Orlandea ²⁸, J.M. Otalora Goicochea ², P. Owen ⁵², B.K. Pal ⁵⁶, A. Palano ^{13,b}, M. Palutan ¹⁸, J. Panman ³⁷, A. Papanestis ⁴⁸, M. Pappagallo ⁵⁰, C. Parkes ⁵³, C.J. Parkinson ⁵², G. Passaleva ¹⁷, G.D. Patel ⁵¹, M. Patel ⁵², G.N. Patrick ⁴⁸, C. Patrignani ^{19,i}, C. Pavel-Nicorescu ²⁸, A. Pazos Alvarez ³⁶, A. Pellegrino ⁴⁰, G. Penso ^{24,l}, M. Pepe Altarelli ³⁷, S. Perazzini ^{14,c}, D.L. Perego ^{20,j}, E. Perez Trigo ³⁶, A. Pérez-Calero Yzquierdo ³⁵, P. Perret ⁵, M. Perrin-Terrin ⁶, G. Pessina ²⁰, K. Petridis ⁵², A. Petrolini ^{19,i}, A. Phan ⁵⁶, E. Picatoste Olloqui ³⁵, B. Pietrzyk ⁴, T. Pilař ⁴⁷, D. Pinci ²⁴, S. Playfer ⁴⁹, M. Plo Casasus ³⁶, F. Polci ⁸, G. Polok ²⁵, A. Poluektov ^{47,33}, E. Polycarpo ², D. Popov ¹⁰, B. Popovici ²⁸, C. Potterat ³⁵, A. Powell ⁵⁴, J. Prisciandaro ³⁸, V. Pugatch ⁴³, A. Puig Navarro ³⁸, G. Punzi ^{22,r}, W. Qian ⁴, J.H. Rademacker ⁴⁵, B. Rakotomiaramanana ³⁸, M.S. Rangel ², I. Raniuk ⁴², N. Rauschmayr ³⁷, G. Raven ⁴¹, S. Redford ⁵⁴, M.M. Reid ⁴⁷, A.C. dos Reis ¹, S. Ricciardi ⁴⁸, A. Richards ⁵², K. Rinnert ⁵¹, V. Rives Molina ³⁵, D.A. Roa Romero ⁵, P. Robbe ⁷, E. Rodrigues ⁵³, P. Rodriguez Perez ³⁶, S. Roiser ³⁷, V. Romanovsky ³⁴, A. Romero Vidal ³⁶, J. Rouvinet ³⁸, T. Ruf ³⁷, F. Ruffini ²², H. Ruiz ³⁵, P. Ruiz Valls ^{35,o}, G. Sabatino ^{24,k},

J.J. Saborido Silva ³⁶, N. Sagidova ²⁹, P. Sail ⁵⁰, B. Saitta ^{15,d}, C. Salzmann ³⁹, B. Sanmartin Sedes ³⁶, M. Sannino ^{19,i}, R. Santacesaria ²⁴, C. Santamarina Rios ³⁶, E. Santovetti ^{23,k}, M. Sapunov ⁶, A. Sarti ^{18,l}, C. Satriano ^{24,m}, A. Satta ²³, M. Savrie ^{16,e}, D. Savrina ^{30,31}, P. Schaack ⁵², M. Schiller ⁴¹, H. Schindler ³⁷, M. Schlupp ⁹, M. Schmelling ¹⁰, B. Schmidt ³⁷, O. Schneider ³⁸, A. Schopper ³⁷, M.-H. Schune ⁷, R. Schwemmer ³⁷, B. Sciascia ¹⁸, A. Sciubba ²⁴, M. Seco ³⁶, A. Semennikov ³⁰, K. Senderowska ²⁶, I. Sepp ⁵², N. Serra ³⁹, J. Serrano ⁶, P. Seyfert ¹¹, M. Shapkin ³⁴, I. Shapoval ^{42,37}, P. Shatalov ³⁰, Y. Shcheglov ²⁹, T. Shears ^{51,37}, L. Shekhtman ³³, O. Shevchenko ⁴², V. Shevchenko ³⁰, A. Shires ⁵², R. Silva Coutinho ⁴⁷, T. Skwarnicki ⁵⁶, N.A. Smith ⁵¹, E. Smith ^{54,48}, M. Smith ⁵³, M.D. Sokoloff ⁵⁹, F.J.P. Soler ⁵⁰, F. Soomro ^{18,37}, D. Souza ⁴⁵, B. Souza De Paula ², B. Spaan ⁹, A. Sparkes ⁴⁹, P. Spradlin ⁵⁰, F. Stagni ³⁷, S. Stahl ¹¹, O. Steinkamp ³⁹, S. Stoica ²⁸, S. Stone ⁵⁶, B. Storaci ³⁹, M. Straticiuc ²⁸, U. Straumann ³⁹, V.K. Subbiah ³⁷, S. Swientek ⁹, V. Syropoulos ⁴¹, M. Szczechowski ²⁷, P. Szczypka ^{38,37}, T. Szumlak ²⁶, S. T'Jampens ⁴, M. Teklishyn ⁷, E. Teodorescu ²⁸, F. Teubert ³⁷, C. Thomas ⁵⁴, E. Thomas ³⁷, J. van Tilburg ¹¹, V. Tisserand ⁴, M. Tobin ³⁹, S. Tolk ⁴¹, D. Tonelli ³⁷, S. Topp-Joergensen ⁵⁴, N. Torr ⁵⁴, E. Tournefier ^{4,52}, S. Tourneur ³⁸, M.T. Tran ³⁸, M. Tresch ³⁹, A. Tsaregorodtsev ⁶, P. Tsopelas ⁴⁰, N. Tuning ⁴⁰, M. Ubeda Garcia ³⁷, A. Ukleja ²⁷, D. Urner ⁵³, U. Uwer ¹¹, V. Vagnoni ¹⁴, G. Valenti ¹⁴, R. Vazquez Gomez ³⁵, P. Vazquez Regueiro ³⁶, S. Vecchi ¹⁶, J.J. Velthuis ⁴⁵, M. Veltri ^{17,g}, G. Veneziano ³⁸, M. Vesterinen ³⁷, B. Viaud ⁷, D. Vieira ², X. Vilasis-Cardona ^{35,n}, A. Vollhardt ³⁹, D. Volyansky ¹⁰, D. Voong ⁴⁵, A. Vorobyev ²⁹, V. Vorobyev ³³, C. Voß ⁵⁸, H. Voss ¹⁰, R. Waldi ⁵⁸, R. Wallace ¹², S. Wandernoth ¹¹, J. Wang ⁵⁶, D.R. Ward ⁴⁶, N.K. Watson ⁴⁴, A.D. Webber ⁵³, D. Websdale ⁵², M. Whitehead ⁴⁷, J. Wicht ^{37,*}, J. Wiechczynski ²⁵, D. Wiedner ¹¹, L. Wiggers ⁴⁰, G. Wilkinson ⁵⁴, M.P. Williams ^{47,48}, M. Williams ⁵⁵, F.F. Wilson ⁴⁸, J. Wishahi ⁹, M. Witek ²⁵, S.A. Wotton ⁴⁶, S. Wright ⁴⁶, S. Wu ³, K. Wyllie ³⁷, Y. Xie ^{49,37}, F. Xing ⁵⁴, Z. Xing ⁵⁶, Z. Yang ³, R. Young ⁴⁹, X. Yuan ³, O. Yushchenko ³⁴, M. Zangoli ¹⁴, M. Zavertyaev ^{10,a}, F. Zhang ³, L. Zhang ⁵⁶, W.C. Zhang ¹², Y. Zhang ³, A. Zhelezov ¹¹, A. Zhokhov ³⁰, L. Zhong ³, A. Zvyagin ³⁷

¹ Centro Brasileiro de Pesquisas Físicas (CBPF), Rio de Janeiro, Brazil² Universidade Federal do Rio de Janeiro (UFRJ), Rio de Janeiro, Brazil³ Center for High Energy Physics, Tsinghua University, Beijing, China⁴ LAPP, Université de Savoie, CNRS/IN2P3, Annecy-Le-Vieux, France⁵ Clermont Université, Université Blaise Pascal, CNRS/IN2P3, LPC, Clermont-Ferrand, France⁶ CPPM, Aix-Marseille Université, CNRS/IN2P3, Marseille, France⁷ LAL, Université Paris-Sud, CNRS/IN2P3, Orsay, France⁸ LPNHE, Université Pierre et Marie Curie, Université Paris Diderot, CNRS/IN2P3, Paris, France⁹ Fakultät Physik, Technische Universität Dortmund, Dortmund, Germany¹⁰ Max-Planck-Institut für Kernphysik (MPIK), Heidelberg, Germany¹¹ Physikalisches Institut, Ruprecht-Karls-Universität Heidelberg, Heidelberg, Germany¹² School of Physics, University College Dublin, Dublin, Ireland¹³ Sezione INFN di Bari, Bari, Italy¹⁴ Sezione INFN di Bologna, Bologna, Italy¹⁵ Sezione INFN di Cagliari, Cagliari, Italy¹⁶ Sezione INFN di Ferrara, Ferrara, Italy¹⁷ Sezione INFN di Firenze, Firenze, Italy¹⁸ Laboratori Nazionali dell'INFN di Frascati, Frascati, Italy¹⁹ Sezione INFN di Genova, Genova, Italy²⁰ Sezione INFN di Milano Bicocca, Milano, Italy²¹ Sezione INFN di Padova, Padova, Italy²² Sezione INFN di Pisa, Pisa, Italy²³ Sezione INFN di Roma Tor Vergata, Roma, Italy²⁴ Sezione INFN di Roma La Sapienza, Roma, Italy²⁵ Henryk Niewodniczanski Institute of Nuclear Physics Polish Academy of Sciences, Kraków, Poland²⁶ AGH University of Science and Technology, Kraków, Poland²⁷ National Center for Nuclear Research (NCBJ), Warsaw, Poland²⁸ Horia Hulubei National Institute of Physics and Nuclear Engineering, Bucharest-Magurele, Romania²⁹ Petersburg Nuclear Physics Institute (PNPI), Gatchina, Russia³⁰ Institute of Theoretical and Experimental Physics (ITEP), Moscow, Russia³¹ Institute of Nuclear Physics, Moscow State University (SINP MSU), Moscow, Russia³² Institute for Nuclear Research of the Russian Academy of Sciences (INR RAN), Moscow, Russia³³ Budker Institute of Nuclear Physics (SB RAS) and Novosibirsk State University, Novosibirsk, Russia³⁴ Institute for High Energy Physics (IHEP), Protvino, Russia³⁵ Universitat de Barcelona, Barcelona, Spain³⁶ Universidad de Santiago de Compostela, Santiago de Compostela, Spain³⁷ European Organization for Nuclear Research (CERN), Geneva, Switzerland³⁸ Ecole Polytechnique Fédérale de Lausanne (EPFL), Lausanne, Switzerland³⁹ Physik-Institut, Universität Zürich, Zürich, Switzerland⁴⁰ Nikhef National Institute for Subatomic Physics, Amsterdam, The Netherlands⁴¹ Nikhef National Institute for Subatomic Physics and VU University Amsterdam, Amsterdam, The Netherlands⁴² NSC Kharkiv Institute of Physics and Technology (NSC KIPT), Kharkiv, Ukraine⁴³ Institute for Nuclear Research of the National Academy of Sciences (KINR), Kyiv, Ukraine

- ⁴⁴ University of Birmingham, Birmingham, United Kingdom
⁴⁵ H.H. Wills Physics Laboratory, University of Bristol, Bristol, United Kingdom
⁴⁶ Cavendish Laboratory, University of Cambridge, Cambridge, United Kingdom
⁴⁷ Department of Physics, University of Warwick, Coventry, United Kingdom
⁴⁸ STFC Rutherford Appleton Laboratory, Didcot, United Kingdom
⁴⁹ School of Physics and Astronomy, University of Edinburgh, Edinburgh, United Kingdom
⁵⁰ School of Physics and Astronomy, University of Glasgow, Glasgow, United Kingdom
⁵¹ Oliver Lodge Laboratory, University of Liverpool, Liverpool, United Kingdom
⁵² Imperial College London, London, United Kingdom
⁵³ School of Physics and Astronomy, University of Manchester, Manchester, United Kingdom
⁵⁴ Department of Physics, University of Oxford, Oxford, United Kingdom
⁵⁵ Massachusetts Institute of Technology, Cambridge, MA, United States
⁵⁶ Syracuse University, Syracuse, NY, United States
⁵⁷ Pontifícia Universidade Católica do Rio de Janeiro (PUC-Rio), Rio de Janeiro, Brazil ^t
⁵⁸ Institut für Physik, Universität Rostock, Rostock, Germany ^u
⁵⁹ University of Cincinnati, Cincinnati, OH, United States ^v

* Corresponding author.

E-mail address: jean.wicht@cern.ch (J. Wicht).

^a P.N. Lebedev Physical Institute, Russian Academy of Science (LPI RAS), Moscow, Russia.

^b Università di Bari, Bari, Italy.

^c Università di Bologna, Bologna, Italy.

^d Università di Cagliari, Cagliari, Italy.

^e Università di Ferrara, Ferrara, Italy.

^f Università di Firenze, Firenze, Italy.

^g Università di Urbino, Urbino, Italy.

^h Università di Modena e Reggio Emilia, Modena, Italy.

ⁱ Università di Genova, Genova, Italy.

^j Università di Milano Bicocca, Milano, Italy.

^k Università di Roma Tor Vergata, Roma, Italy.

^l Università di Roma La Sapienza, Roma, Italy.

^m Università della Basilicata, Potenza, Italy.

ⁿ LIFAELS, La Salle, Universitat Ramon Llull, Barcelona, Spain.

^o IFIC, Universitat de Valencia-CSIC, Valencia, Spain.

^p Hanoi University of Science, Hanoi, Viet Nam.

^q Università di Padova, Padova, Italy.

^r Università di Pisa, Pisa, Italy.

^s Scuola Normale Superiore, Pisa, Italy.

^t Associated to: Universidade Federal do Rio de Janeiro (UFRJ), Rio de Janeiro, Brazil.

^u Associated to: Physikalisches Institut, Ruprecht-Karls-Universität Heidelberg, Heidelberg, Germany.

^v Associated to: Syracuse University, Syracuse, NY, United States.